

Rutile solubility in supercritical NaAlSi₃O₈–H₂O fluids

Leslie A. Hayden^{*,1}, Craig E. Manning

Department of Earth and Space Sciences, University of California Los Angeles, Los Angeles CA 90095, USA

ARTICLE INFO

Article history:

Received 22 September 2010
Received in revised form 7 February 2011
Accepted 8 February 2011
Available online 18 February 2011

Editor: D.B. Dingwell

Keywords:

Rutile solubility
Supercritical fluids
Ti mobility
Subduction zones
Albite

ABSTRACT

Rutile solubility was measured in the supercritical NaAlSi₃O₈–H₂O system using hydrothermal piston–cylinder methods at 900 °C. Solubility in intermediate albite–H₂O fluids varies as a function of both pressure (*P*) and fluid composition (*X*). Rutile solubility increases with increased albite content of the fluid, and is on the order of ~1000 to ~5000 ppm for all *P*–*X* conditions investigated here. The relationship between solubility and pressure is complex, and solubility decreases with increasing pressure for intermediate fluid compositions (35–75 wt.% H₂O). Ti contents of glasses indicate that, with rising pressure at 900 °C, the liquid–vapor miscibility gap in the albite–H₂O system closes at 0.9–1.0 GPa. A single supercritical fluid is stable above this pressure, to 2.0–2.2 GPa when further compression induces a return to a subcritical state. Supercritical fluids could be plausible transfer agents for Ti and other HFSE in high-*P* metamorphic environments, but the results show that their stability may be more limited than previously recognized.

© 2011 Elsevier B.V. All rights reserved.

1. Introduction

Rutile (TiO₂) is a ubiquitous accessory mineral in igneous, metamorphic and sedimentary rocks. One of its importances lies in its ability to accommodate high-field-strength elements (HFSE), making it an important monitor of processes such as element cycling, melt evolution, and subduction zone metasomatism (e.g., Ryerson and Watson, 1987; Ayers and Watson, 1991, 1993; Brenan et al., 1994; Rudnick et al., 2000; Zack et al., 2002). With rutile playing a crucial role in a wide range of geological processes, it is essential to have a comprehensive understanding of its geochemical behavior, including its relationship with geologic fluids.

It was long believed that rutile had very limited solubility in most types of aqueous fluids encountered in geologic settings. Rutile is a common residual mineral during hydrothermal alteration (Force, 1991), and early experimental investigation yielded low rutile solubility in H₂O-rich fluids at intermediate temperature (*T*) and pressure (*P*) (Schuiling and Vink, 1967). However, more recent work suggests that under conditions such as those found in high-*P* metamorphic environments, rutile may exhibit elevated solubility in aqueous fluids (Ayers and Watson, 1993; Audétat and Keppler, 2005; Tropper and Manning, 2005; Antignano and Manning, 2008; Manning et al., 2008),

which will result in enhanced Ti mobility (Van Baalen, 1993; Jiang et al., 2005). In contrast, rutile solubility in silicate liquids ± H₂O may be up to several orders of magnitude higher at a given *P* and *T* (Ryerson and Watson, 1987; Hayden and Watson, 2007; Spandler et al., 2007; Gaetani et al., 2008).

It has been proposed that silicate–H₂O systems of intermediate composition form a single, supercritical fluid phase that may enhance the transport of otherwise immobile trace elements (e.g., Manning, 2004; Kessel et al., 2005a, 2005b; Hermann et al., 2006; Hermann and Spandler, 2008; Klimm et al., 2008). Supercritical fluids occur at *P* and *T* at which there is complete miscibility between a hydrous silicate liquid and an H₂O-rich vapor phase. For example, the simple H₂O–NaAlSi₃O₈ (albite) system exhibits this behavior over a range of geologically relevant pressures and temperatures (Fig. 1). Such critical mixing is achieved when, for a given bulk composition, the dissolved constituents can evolve continuously from ions and isolated molecules to a polymerized silicate network as rock components are added to H₂O (e.g., Manning, 2004; Manning et al., 2010). Supercritical fluids are potentially important in high-*P* environments, and it is likely that such fluids are powerful solvents for refractory trace components, such as Ti or other HFSE. However, there has been no systematic study of the change in solubility of a mineral or element in a supercritical fluid with *P* or *T* over a wide range of H₂O contents. To address this issue, we experimentally investigated rutile solubility in supercritical H₂O–albite, ranging from ~30 to ~75 wt.% H₂O and 0.9 to 2.2 GPa at 900 °C (Fig. 1). In addition to characterizing the roles of *P* and H₂O content on Ti concentration at rutile saturation, the work also offers new insights into the phase relations in this simple but petrologically important binary system.

* Corresponding author.

E-mail addresses: lahayden@umich.edu (L.A. Hayden), manning@ess.ucla.edu (C.E. Manning).

¹ Present address: Department of Geological Sciences, University of Michigan, 2534 C.C. Little Bldg., 1100 N. University Ave., Ann Arbor MI 48109.

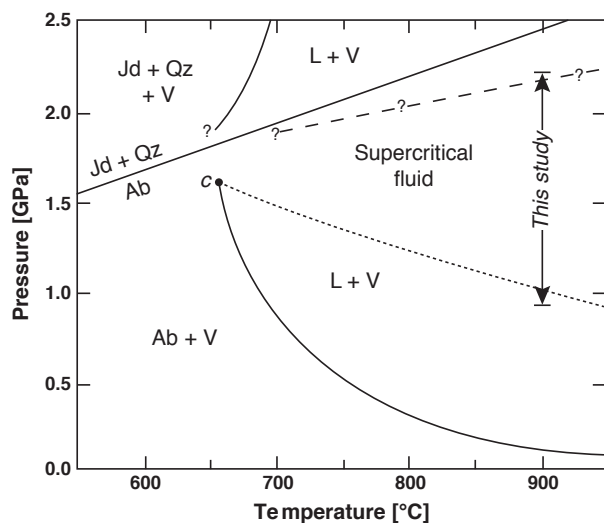


Fig. 1. *P*–*T* diagram illustrating phase relations in the albite–H₂O system. Abbreviations: Ab, albite; Jd, jadeite; Qz, quartz; L, liquid; V, vapor; c, critical end point. Phase relations after Boettcher and Yllie (1969), Goldsmith and Jenkins (1985), Shen and Keppler (1997), Holland and Powell (1998, 2002 update), Stadler et al. (2000), and this study. Albite or jadeite + quartz coexist with a single, fluid phase at *P* and *T* higher than the crest of the L + V miscibility (short-dash line). The existence of an H₂O-saturated solidus in the Jd + Qz stability field (Boettcher and Yllie, 1969) implies the reappearance of an L + V field at high *P* (long-dash line). The *P* range over which this study measured rutile solubility is shown by the arrow at 900 °C. The data are consistent with the upper boundary of the supercritical fluid field as depicted here, but suggest the lower boundary lies at <0.9 GPa at 900 °C (see text).

2. Methods

The starting material was a synthetic albite (NaAlSi₃O₈) glass from a stoichiometric mix of oxides (Al₂O₃ and SiO₂) and Na₂CO₃. The mixture was ground under ethanol, placed in a clean Pt crucible, and fused in a tube furnace at 1250 °C for 24 h. This procedure was repeated twice to ensure a homogenous starting material. For experiments SC2–SC39 (Table 1), the albite glass was ground into a fine powder, mixed with 2 wt.% TiO₂ powder (Aesar), then reground. For each of these experiments, the glass–TiO₂ mix powder was weighed and loaded into a 1.6 mm OD Pt capsule. For experiments SC40–SC45, an aliquot of the Ti-free albite glass was used along with a pure synthetic rutile crystal as the source of Ti (these experiments utilized the same pure synthetic rutile as the study of Tropper and Manning (2005) and Antignano and Manning (2008)). For these experiments, a single rutile crystal large enough to ensure saturation was added to a 1.6 mm OD Pt capsule, which was then loaded with powdered Ti-free albite glass. For all experiments, distilled, deionized H₂O was then added to the Pt capsules with a syringe, the Pt capsule was weighed again, crimped shut, sealed by arc-welding and then weighed again (to insure no loss of H₂O had occurred). The capsule was then placed in a 115 °C oven for 1 h to check for leakage, and any incompletely sealed capsules (as noted by weight loss) were discarded. The albite, water, and Pt capsules were weighed with a Mettler M3 microbalance (1σ = 2 μg).

The experiments were conducted in a piston–cylinder apparatus using 2.54-cm NaCl–graphite assemblies (Manning, 1994; Manning and Boettcher, 1994). All experiments were run at 900 °C and at pressures ranging from 0.9–2.2 GPa. Temperature was controlled with calibrated Pt–Pt₁₀Rh₉₀ thermocouples with an estimated accuracy of ±3 °C; no correction was made for the effect of emf on temperature. Pressure was monitored with a Heise gage and held to within 200 bar (0.02 GPa) of the target pressure. Experiments were held at temperature and pressure for a minimum of 20 h. Rapid quenching to <50 °C within 1 min was achieved by cutting power to the apparatus.

Table 1
Conditions and results of experiments at 900 °C.

Experiment number	<i>P</i> (GPa)	Duration (h)	Albite glass ± 2 wt.% TiO ₂ (mg)	H ₂ O (mg)	Bulk H ₂ O** (wt.%)	Ti solubility (ppm)
SC-35	0.9	24	2.058	1.603	43.79	3762(65)
SC-36	0.9	25	1.916	3.017	61.16	3593(65)†
SC-37	0.9	25	1.506	3.042	66.89	3184(67) †
SC-40*	0.9	42	2.963	1.407	32.20	3785(65)
SC-41*	0.9	42	2.756	1.736	38.65	3755(66)
SC-42*	0.9	24	2.148	2.139	49.90	3771(65)
SC-43*	0.9	24	1.986	2.427	55.00	3684(67)
SC-26	1.0	48	2.009	1.704	45.89	3470(68)
SC-27	1.0	48	2.633	1.946	42.50	3572(67)
SC-28	1.0	24	2.994	1.303	30.32	3763(67)
SC-29	1.0	24	2.406	2.302	48.90	3417(68)
SC-30	1.0	24	3.607	4.567	55.87	3299(67)
SC-31	1.0	27	3.015	4.623	60.53	2963(75)
SC-32	1.0	27	1.571	3.310	67.81	2271(94)
SC-21	1.25	25	1.537	0.917	37.37	3611(78)
SC-22	1.25	25	1.500	2.155	58.96	2517(91)
SC-23	1.25	25	3.029	2.040	40.24	3541(77)
SC-24	1.25	24	2.178	1.713	44.02	3354(78)
SC-25	1.25	24	2.633	2.809	51.62	2984(86)
SC-33	1.25	39	2.631	2.462	48.34	3213(85)
SC-34	1.25	39	2.457	2.975	54.77	2779(91)
SC-2	1.5	68	3.529	1.840	34.27	2975(104)
SC-3	1.5	70	4.460	1.440	24.41	4811(61)
SC-4	1.5	70	4.079	2.554	38.50	2748(96)
SC-5	1.5	28	0.932	0.858	47.93	2610(91)
SC-6	1.5	28	1.842	2.707	59.51	2391(84)
SC-9	1.5	44	1.418	2.632	64.99	2011(90)
SC-10	1.5	44	0.787	2.281	74.35	1117(150)
SC-11	1.5	44	2.741	1.084	28.34	4217(60)
SC-12	1.5	48	1.857	1.237	39.98	2769(90)
SC-13	1.5	48	1.441	1.184	45.10	2631(90)
SC-14	1.5	26	2.586	2.634	50.46	2610(91)
SC-15	1.5	26	1.631	2.107	56.37	2472(91)
SC-16	1.5	26	1.204	2.416	66.74	1931(110)
SC-17	2.0	24	3.884	1.516	28.07	1958(91)
SC-18	2.0	24	1.213	2.758	69.45	1687(128)
SC-19	2.0	23	2.459	1.624	39.77	1887(127)
SC-20	2.0	23	1.701	2.042	54.56	1754(128)
SC-38	2.2	20	3.016	1.231	28.99	1759(141)
SC-39	2.2	22	2.664	2.873	51.89	1742(140)
SC-44*	2.2	20	2.763	1.738	38.61	1755(140)
SC-45*	2.2	22	1.615	2.998	64.99	1690(140)

Explanation: 1σ weighing errors are 2 μg. Ti solubility determined by electron probe microanalyses of quench glass. Parenthetical numbers represent analytical uncertainty (1σ) in final digits.

*These experiments featured a Ti-free starting albite glass. A single synthetic rutile crystal was used as the TiO₂ source; the mass was sufficient to maintain rutile saturation, but it is not included with the glass weight.

†These experiments were likely run within the two-phase field and do not represent equilibrium values. See Fig. 8 and Sections 3.3 and 4.4 for further discussion.

**Bulk H₂O refers to wt% H₂O relative to total added glass ± TiO₂ powder. It is the minimum H₂O content of the fluid because any new rutile crystals are neglected (see text).

Capsules were removed from the furnace assembly, weighed again to ensure that the integrity of the capsule was maintained during the run, then sliced open with a razor blade and dried at 115 °C for several minutes. In the experiments featuring the albite glass–TiO₂ mix, the run products were inspected with an optical microscope and then mounted in epoxy and polished. In the experiments featuring a rutile single crystal, the crystal was removed from the capsule and the remaining capsule contents were inspected with an optical microscope and then mounted in epoxy and polished.

Quenched glass run products were imaged using backscattered electron microscopy, and analyzed with a JEOL JXA-8200 electron microprobe. Operating conditions included a 15 keV accelerating potential and a 10 nA current, with a 5 μm spot size. This relatively low current and broad beam was necessary to minimize mobility of Na during analysis and prevent excessive damage to the water-rich

quench glass, which is very fragile under an electron beam. Counting times for acquisition were 10 s for Na, 20 s for Si and Al and 60 s for Ti. X-ray counts for Na were monitored to ensure that they remained constant and did not decrease due to Na volatility. These conditions resulted in a detection limit of ~700 ppm for Ti, which was acceptable for these samples. Because of the secondary fluorescence behavior of Ti, glasses were analyzed at a minimum distance of ~50 μm from any visible rutile crystals, to prevent interference from the rutile that would contaminate the Ti analyses.

3. Results

3.1. Run products

All experiments returned quench glasses that largely filled the capsule volume, texturally implying the presence of a single fluid phase during these experiments. We noted a spectrum of preserved states of the glasses, from large irregular fragments to minute, angular to rounded pieces. The most common texture is medium to large, irregular glass fragments that may be tens of microns to millimeters in the longest dimension (Fig. 2). The pieces are variably vesiculated, ranging from apparently bubble free to bubble rich. In some run products, bubble rich and bubble free zones occur within the same fragments. Most glass pieces were angular, implying fracturing in the solid state; however, in some cases the quench products also include small glass spherules and locally rounded edges. We observed no systematic variation in these textures with bulk H_2O content or pressure.

The other extreme of quench textures was voluminous, minute glassy particles (Fig. 3). Both spherulitic to irregularly rounded objects and angular pieces may occur. The size range is from ~1 to ~50 μm . This texture may be observed at any pressure; however, with one exception (SC-35), all experiments at 0.9 and 2.2 GPa display this type

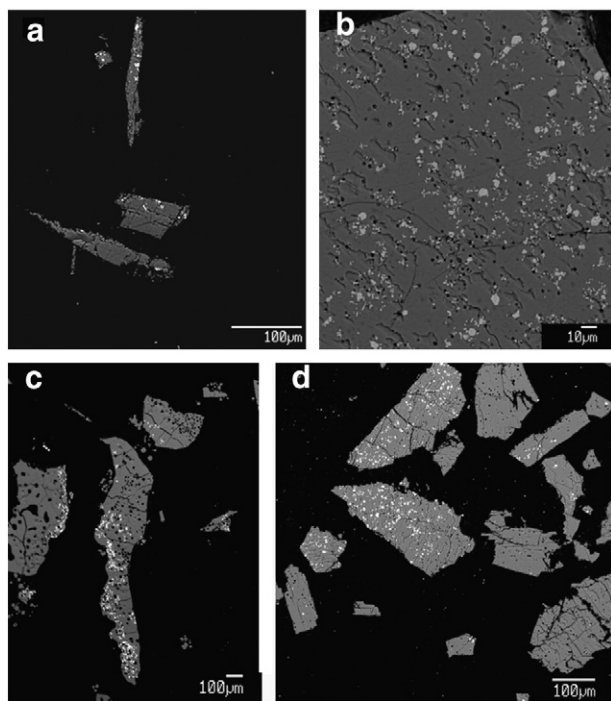


Fig. 2. Backscattered electron images of selected experiments featuring large, irregular fragments of quench glasses. All contain visible, disseminated, newly formed rutile crystals. (a) SC27, 1 GPa, 42 wt.% H_2O ; (b) SC14, 1.5 GPa, 50 wt.% H_2O ; (c) SC30, 1 GPa, 56 wt.% H_2O ; (d) SC21, 1.25 GPa, 37 wt.% H_2O .

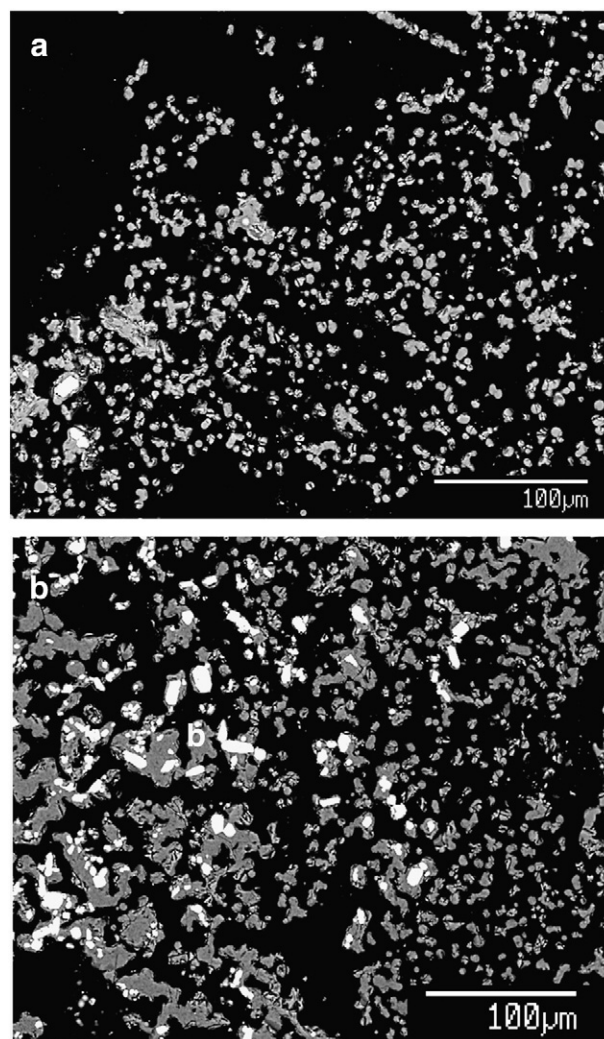


Fig. 3. Backscattered electron images of selected experiments featuring minute glassy particles. Textures range from rounded to angular; rutile crystals occur in many pieces. (a) SC39, 2.2 GPa, 52 wt.% H_2O ; (b) SC36, 0.9 GPa, 61 wt.% H_2O .

of quench texture. Explanations for the contrasting quench textures are considered below in Section 3.5.

Regardless of quench texture, equant, rutile crystals up to ~10 μm in the longest dimension occur within the glasses (Figs. 2 and 3). In cases where only small particles are present, many pieces do not contain rutile (Fig. 3).

The run products contained no other residual phases (e.g., corundum or paragonite) that would suggest incongruent albite dissolution, in contrast to the residual phases present in the run products of Antignano and Manning (2008), which contained significantly less dissolved silicate. During these experiments, the rutile crystals underwent a change in color from translucent, pale yellow to deep blue-black. This is the result of trace reduction of Ti^{4+} to Ti^{3+} , in conjunction with charge-compensating H^+ substitution (Colasanti et al., 2007).

3.2. Equilibrium

Experiments at similar H_2O content and identical pressures indicated that constant Ti concentration, assumed to indicate equilibrium, was attained after a period of ~24 h (Fig. 4). Experiments were therefore run for a minimum of 20 h (Table 1). Equilibrium was approached from undersaturation in all cases.

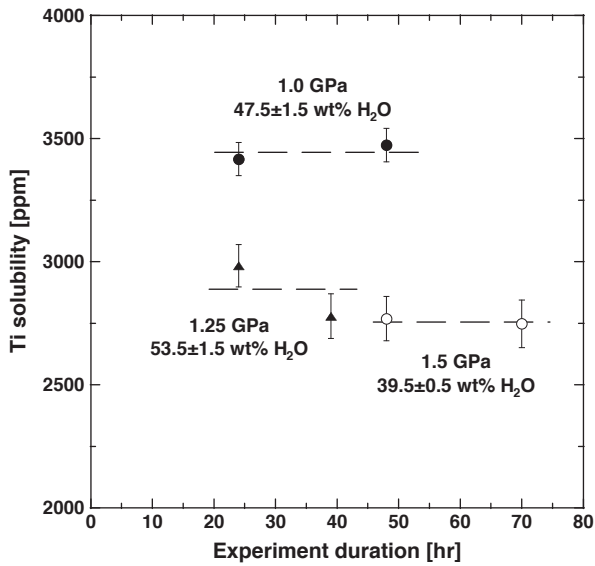


Fig. 4. Rutile solubility as a function of experiment duration at three different P–T conditions. The absence of detectable change with time supports the interpretation of attainment of equilibrium. All experiments were run for a minimum of 20 h to ensure equilibrium.

3.3. H₂O content of glasses

The run-product glasses display a wide range in vesicularity, suggesting variable loss of dissolved H₂O during quench. In principle, the amount of H₂O in the quench glasses can be estimated from the difference between the oxide sum and 100% (e.g., Baker, 2004). If a supercritical, one-phase fluid was present during an experiment, then the estimated H₂O content should agree with the bulk H₂O of the experiment only if the extent of H₂O exsolution is small. Table 2 compares H₂O concentration determined by both methods. The H₂O estimated by difference is in every case higher than the bulk value, with an average deviation of 2.2 wt.%. In experiments utilizing albite glass + 2% TiO₂ powder, bulk H₂O is up to 2 wt.% lower than the equilibrium melt value because rutile grown during an experiment is not taken into account. Thus, Table 2 nominally indicates good agreement between expected and estimated H₂O contents over the entire range of conditions investigated.

There are two possible explanations for the agreement between the different H₂O determinations in Table 2. It could be that H₂O loss via vesiculation is indeed minor, and that there is no systematic variation in preserved H₂O content, regardless of quench texture. In this scenario, H₂O determined by difference reflects dissolved H₂O in the melt at high P and T, and the determined H₂O contents signify supercritical conditions at all investigated P and T. The second possibility is that analyzed glasses were vesiculated at the submicron scale. In this case the lower analytical totals would result from microporosity rather than dissolved H₂O. In this case, the H₂O content at high P and T is indeterminate, and it does not constrain supercritical or subcritical behavior.

3.4. Rutile solubility

Titanium concentrations in the quenched glasses are given in Tables 1 and 2 and shown in Fig. 5. Rutile solubilities vary from ~1000 to ~5000 ppm Ti over the conditions investigated. The data constrain six rutile solubility isobars at 900 °C. At 1.25 and 1.5 GPa, rutile solubility isobars show a strong, sigmoidal dependence on the H₂O content of the fluid (Fig. 5). Ti solubility at these P is greatest in low-H₂O fluids. It decreases with rising H₂O content, but in the middle of the compositional range the slope is shallower than at the highest and

Table 2
Electron microprobe microanalyses of rutile-saturated glasses.

	SC-2	SC-3	SC-4	SC-5	SC-6	SC-9	SC-10	SC-11	SC-12
SiO ₂	42.70	49.17	39.46	33.64	25.88	22.64	16.82	46.58	38.82
TiO ₂	0.496	0.803	0.458	0.435	0.399	0.335	0.186	0.703	0.462
Al ₂ O ₃	12.89	14.85	11.92	10.16	7.81	6.84	5.08	14.07	11.72
Na ₂ O	7.09	8.16	6.55	5.59	4.30	3.76	2.79	7.74	6.45
H ₂ O*	34.27	24.41	38.50	47.93	59.51	64.99	74.35	28.34	39.98
Total	97.45	97.39	96.90	97.75	97.90	98.56	99.23	97.42	97.43
H ₂ O**	36.82	27.02	41.61	50.18	61.61	66.42	75.12	30.92	42.55
	SC-13	SC-14	SC-15	SC-16	SC-17	SC-18	SC-19	SC-20	SC-21
SiO ₂	35.58	32.35	28.55	21.41	46.44	20.00	38.70	29.12	40.77
TiO ₂	0.439	0.435	0.412	0.322	0.327	0.281	0.315	0.293	0.602
Al ₂ O ₃	10.75	9.77	8.55	6.42	14.03	6.04	11.69	8.76	12.27
Na ₂ O	5.91	5.37	4.77	3.58	7.80	3.36	6.50	4.90	6.85
H ₂ O*	45.10	50.46	56.37	66.74	28.07	69.45	39.77	54.56	37.37
Total	97.78	98.38	98.65	98.47	96.68	99.13	96.99	97.63	97.86
H ₂ O**	47.33	52.08	57.72	68.27	31.40	70.32	42.79	56.93	39.51
	SC-22	SC-23	SC-24	SC-25	SC-26	SC-27	SC-28	SC-29	SC-30
SiO ₂	26.53	38.83	36.16	31.00	34.87	37.46	45.21	32.94	28.42
TiO ₂	0.42	0.591	0.559	0.498	0.579	0.596	0.628	0.57	0.55
Al ₂ O ₃	7.98	11.68	11.34	9.72	10.39	11.16	13.47	9.82	8.47
Na ₂ O	4.46	6.53	6.02	5.16	5.80	6.23	7.52	5.48	4.73
H ₂ O*	58.96	40.24	44.02	51.62	45.89	42.50	30.32	48.90	55.87
Total	98.35	97.87	98.11	97.99	97.54	97.95	97.15	97.70	98.03
H ₂ O**	60.61	42.37	45.92	53.63	48.35	44.55	33.17	51.20	57.84
	SC-31	SC-32	SC-33	SC-34	SC-35	SC-36	SC-37	SC-38	SC-39
SiO ₂	25.23	20.70	33.64	29.11	36.14	25.28	21.19	40.91	26.91
TiO ₂	0.494	0.379	0.536	0.464	0.628	0.599	0.531	0.293	0.291
Al ₂ O ₃	7.66	6.28	10.21	8.83	10.99	7.58	6.42	15.00	10.56
Na ₂ O	4.19	3.44	5.59	4.83	5.96	4.19	3.55	10.12	6.77
H ₂ O*	60.53	67.81	48.34	54.77	43.79	61.16	66.89	28.99	51.89
Total	98.10	98.61	98.31	98.01	97.51	98.81	98.57	95.30	96.41
H ₂ O**	62.43	69.20	50.03	56.76	46.28	62.35	68.32	33.68	55.47
	SC-40	SC-41	SC-42	SC-43	SC-44	SC-45			
SiO ₂	43.88	39.36	32.36	29.12	35.91	18.96			
TiO ₂	0.631	0.626	0.629	0.615	0.293	0.282			
Al ₂ O ₃	13.35	11.98	9.82	8.83	13.53	7.44			
Na ₂ O	7.24	6.49	5.28	4.75	9.24	4.77			
H ₂ O*	32.20	38.65	49.90	55.00	38.61	64.99			
Total	97.30	97.11	97.97	98.31	97.58	96.44			
H ₂ O**	34.90	41.54	51.92	56.68	41.04	68.55			

Explanation: Glass compositions represent averages of 10–12 individual analyses. H₂O* is bulk H₂O in the experiment (Table 1); H₂O** is H₂O concentration calculated by difference from oxide totals, assuming oxide sum is 100%. Average difference between H₂O* and H₂O** is 2.3%.

lowest H₂O contents of the investigated range. At higher and lower P, rutile solubility shows less dependence on H₂O except at its highest concentrations. Thus, the topology of solubility isobars at intermediate H₂O concentrations (30–70 wt.% H₂O) changes with pressure, such that at low P (0.9 GPa) it is nearly flat, but as P increases to 1.0 and then to 1.25 GPa, the curve steepens as dependence on H₂O increases. With further rise in P to 1.5 and 2.0 GPa the solubility isobar progressively shallows until finally, at 2.2 GPa, it is again flat signaling no detectable dependence on H₂O over a wide compositional range.

At fixed, intermediate H₂O concentrations, rutile solubility decreases with increasing P (Fig. 6). Experiments run over a range of pressures at near identical fluid compositions (~40, ~55, and ~67 ± 2.5 wt.% H₂O) show that an increase in P from 0.9 to 2.2 GPa results in a roughly two-fold decrease in Ti solubility; however, the data also show that the decrease in Ti solubility with P is highly non-linear. The greatest change in solubility with pressure is observed at the highest H₂O contents and the lowest P. Rutile solubilities at the highest H₂O concentrations (70 ± 5 wt.%) suggest convergence similar values independent of P.

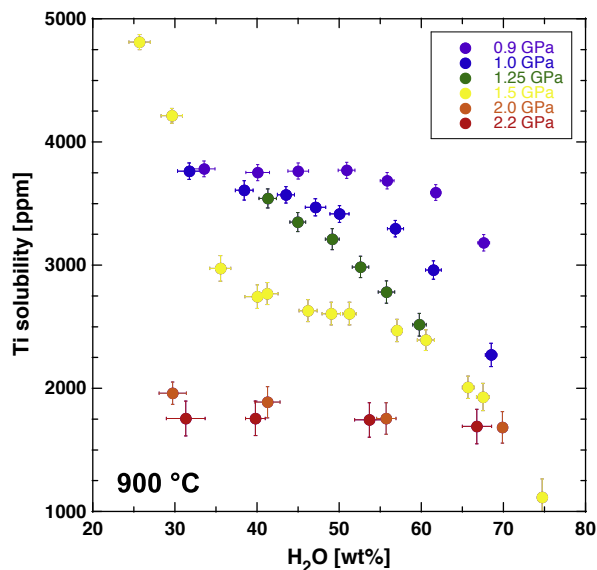


Fig. 5. Rutile solubility in supercritical NaAlSi₃O₈–H₂O fluids at 900 °C. H₂O contents are plotted at the midpoint between bulk H₂O (Table 1) and H₂O in glass determined by difference (Table 2), with the range between these values indicated by the error bars. Uncertainty in Ti concentration reflects 1σ (Table 1). Ti solubility decreases with *P* at fixed fluid composition. It is a non-linear function of fluid composition, showing the greatest dependence on H₂O content at 1.0–1.5 GPa. At 0.9 and 2.2 GPa, Ti solubility is independent of H₂O, signaling proximity to the crest of the miscibility gap in the system albite–H₂O (see text).

3.5. Supercritical behavior of albite–H₂O fluid

Although interpretation of the H₂O contents of the glasses may be ambiguous, the Ti concentrations provide constraints on whether one or two fluid phases are stable at an investigated pressure. If only one fluid phase was present, Ti concentration in quenched glasses should decrease continuously with increasing H₂O. This behavior is observed between 1.0 and 2.0 GPa, suggesting supercritical behavior of rutile-saturated albite–H₂O at these *P*. On the other hand, if two fluid phases were present at any *P*, Ti content must be constant in

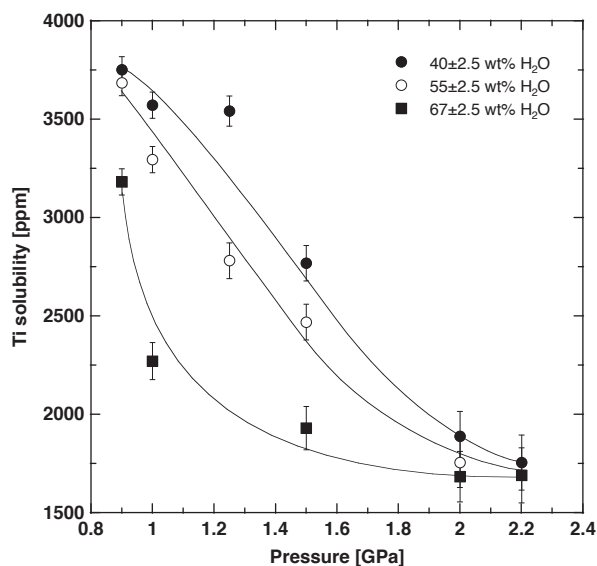


Fig. 6. Rutile solubility as a function of pressure at fixed fluid composition (40, 55, and 67 ± 2.5 wt.% H₂O). Solubility decreases nonlinearly with increasing *P*, with the largest drop found at lower *P* in H₂O-rich compositions.

the melts quenched over a range in bulk H₂O. The Ti concentration is roughly constant within our detection limits at 0.9 and 2.2 GPa (Fig. 5), suggesting that two fluid phases are present at these *P*. Two caveats are, first, that uncertainties in Ti are sufficient to admit a slight non-zero slope over the range of H₂O investigated, and second, that H₂O is not constant (Table 2); however, in light of concerns about preservation of H₂O content the latter is probably not a strong constraint. Thus, the observations imply that at 900 °C, two fluids – a hydrous liquid and a silicate-rich vapor phase are present in the albite–H₂O system below 0.9–1.0 GPa, and above 2.0–2.2 GPa. This interpretation is supported by the prevalence of very fine quench particles at 0.9 and 2.2 GPa. However, quench textures are evidently inconsistent, and the lack of any consistent quench texture as a function of pressure or bulk H₂O suggests that quench paths and processes depend on uncontrolled variables, such as the flow rate of cooling H₂O, the shape and texture of the capsule walls, or the distribution of crystals in the charge.

4. Discussion

4.1. Comparison to previous work at 1 GPa

The new rutile solubility data are the first for intermediate, supercritical albite–H₂O fluids. Previous investigations focused on rutile solubility at 900 °C and 1 GPa, in fluids either more silicate-rich or more H₂O-rich than those of this study (Hayden and Watson, 2007; Antignano and Manning, 2008). Antignano and Manning (2008) determined rutile solubility by single-crystal weight-loss methods. They studied lower dissolved silicate content by adding small quantities of albite glass, in the range 65–100 wt.% H₂O. They found a nearly linear increase in Ti concentration with rising silicate content. Hayden and Watson (2007) investigated rutile solubility in a range of hydrous siliceous melt compositions by equilibrating the melts with a synthetic rutile crystal. The H₂O concentrations were 7–9 wt.% at 900 °C, and 1 GPa.

The Hayden and Watson (2007) study did not examine the pure albite–H₂O system, but their data do include a high-Na trondhjemite, which probably serves as a reasonable proxy for NaAlSi₃O₈ for the sake of comparison. They found no detectable dependence of rutile solubility on H₂O content over the restricted range investigated. Their compositional model (their Eq. 3) predicts rutile solubility of 4206 ppm Ti in albite melt at 900 °C and 1 GPa.

Fig. 7 compares the results of the three studies. There is good agreement that Ti concentration at rutile saturation increases with decreasing H₂O, and although there is only limited overlap in the compositional range, the trends in the data sets are broadly consistent. In particular, the trondhjemite and predicted albite composition of Hayden and Watson (2007) agree closely with the value extrapolated from the data of the present work (Fig. 7). Moreover, solubility change with H₂O in H₂O-poor melts must be comparatively limited, suggesting that the apparent absence of a dependence on H₂O inferred by Hayden and Watson (2007) simply reflects the more restricted compositional range of their investigation.

The combined data sets confirm that rutile solubility decreases sigmoidally with increasing H₂O. The inflection in the solubility curve occurs at ~65 wt.% H₂O. The rutile solubility in the most H₂O-poor composition investigated by Antignano and Manning (2008) is significantly lower than that implied by the present data set. Moreover, three of their experiments at the most silicate-rich compositions were in the two-phase, melt + vapor field, whereas evidence in our run products points to a one-phase fluid at 1.0 GPa. A notable difference is that Antignano and Manning found residual corundum, implying that silicate in the melt + fluid had shifted off albite composition. Nevertheless, in light of the different experimental approaches and compositions, the broad agreement between this work,

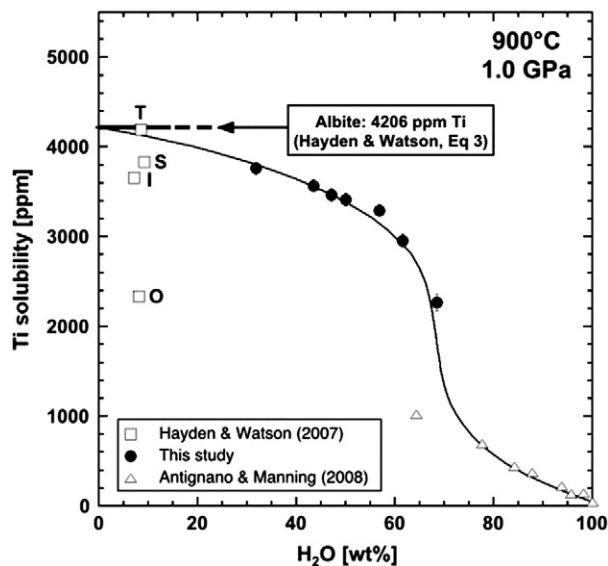


Fig. 7. Comparison of 1 GPa data with previous work at 900 °C. Antignano and Manning (2008, triangles) found evidence for melt + vapor immiscibility in the three most H₂O-poor runs; however, residual corundum suggests that the fluid composition was slightly shifted off the albite–H₂O binary (see text), and the 900 °C data of Hayden and Watson (2007, squares) are for trondhjemite (T), S-type granite (S), intermediate mix (I) and Lake County obsidian (O). The bold, horizontal line corresponds to predicted, H₂O-independent rutile solubility in albite melt using their Eq. 3. Uncertainties as in Fig. 5.

Hayden and Watson (2007), and Antignano and Manning (2008) is encouraging.

4.2. Mechanism of rutile dissolution

Comparison of the results of the present study with those in more H₂O-rich fluids yields insights into the mechanism of rutile dissolution and Ti incorporation in supercritical albite–H₂O. Rutile solubility in H₂O is relatively low (Audétat and Keppler, 2005; Tropper and Manning, 2005; Antignano and Manning, 2008), and most studies indicate rising solubility with an isothermal *P* increase (c.f., Ayers and Watson, 1991). Addition of ~6 wt.% dissolved silicate of approximately albite stoichiometry increases rutile solubility at any *P* and *T*. The increase in solubility with dissolved silicate is roughly linear over this narrow compositional range, and the *P* dependence of the dissolution reaction is the same as in pure H₂O (Antignano and Manning, 2008). However, at the higher dissolved albite concentrations of the present study (~30–70 wt.% H₂O), the dependence of rutile solubility on fluid composition is highly non-linear (Fig. 5), and the dependence on *P* changes such that Ti content at fixed bulk composition and *T* decreases on compression.

In pure H₂O, Ti is incorporated into the fluid chiefly as a hydrated neutral molecule. Increasing rutile solubility with *P* at constant *T* indicates that the standard volume change of rutile dissolution to the aqueous hydrate (e.g., H₄TiO₄) is negative. This is consistent with other oxide dissolution reactions (Dolejš and Manning, 2010). A strong increase in rutile solubility with dissolved Na, Al, and Si at constant *P* and *T* indicates that Ti forms complexes with these added constituents, and that these complexes are substantially more stable than the Ti hydrate. These solutes could take several possible forms.

Alkali–Ti complexes likely serve as one mechanism for rutile solubility enhancement. In felsic melts, rutile solubility increases with both (Na + K)/Al (Dickinson and Hess, 1985; Ryerson and Watson, 1987) and Na/K (Hayden, 2007). Ti is believed to be in five-fold coordination in simple Na₂O–TiO₂–SiO₂ or K₂O–TiO₂–SiO₂ melts (Farges et al., 1996; Henderson et al., 2003). Similarly, in these fluids, ^vTi could be present as NaOTi(OH)₄[−] complexes (Antignano and

Manning, 2008). The presence of dissolved Al also strongly influences rutile solubility. In melts, rutile solubility is enhanced once a melt transitions to an alumina-undersaturated state (Hayden and Watson, 2007; Hayden, 2007). In this case, titanate complexes with mono- and divalent cations present in excess of that required to charge balance Al³⁺ in 4-fold coordination (Mysen et al., 1980). Recent studies suggest that Al–silicate, Na–Al–silicate and K–Al–silicate clusters form in aqueous solutions at high *P* and *T*, featuring Al and Si in tetrahedral coordination (Manning, 2004, 2007; Newton and Manning, 2007, 2008; Mibe et al., 2008). Thus, the substitution of Ti for ^{IV}Al or ^{IV}Si in fluids could also yield tetrahedral coordination of Ti.

The nonlinear dependence of rutile solubility on fluid bulk composition at a given *P* and *T* indicates that the Ti complexes are hydrated, but that there is probably a complex interplay between changing extent of hydration and H₂O activity in the bulk solvent. The change in the isothermal *P* dependence of rutile solubility (from increasing to decreasing Ti with rising *P* as albite concentration increases) implies that the Na ± Al ± Si complexes are large in volume relative to the neutral hydrate.

4.3. Implications for the albite–H₂O phase diagram

Fig. 1 shows phase relations in the albite–H₂O system as a function of *P* and *T*. Previous results suggest that the H₂O-saturated melting curve (Goldsmith and Jenkins, 1985) intersects the curve tracing the crest of the liquid + vapor miscibility gap (Shen and Keppler, 1997) at ~650 °C and 1.5 GPa, forming a critical end point. The data of Boettcher and Wylie (1969) constrain H₂O-saturated melting of jadeite + quartz at 650° and 1.8 GPa. Their results show that the melting curve continues to higher *P* and *T* (Fig. 1). It is possible that the curve also continues to lower *P* and *T*, but their data do not establish with certainty whether it intersects the albite = jadeite + quartz equilibrium. Nevertheless, vapor-saturated melting in the jadeite + quartz stability field requires the stable existence of a liquid + vapor field at these *P*. This in turn implies that the system possesses a second critical curve marking the transition of supercritical fluid to liquid + vapor on compression.

The rutile solubility data constrain three aspects of the albite–H₂O phase relations: (1) the existence of a stable supercritical fluid field over a wide *P* range at 900 °C; (2) the *P* of closure of the L–V miscibility gap in the albite stability field; and (3) the *P* of a return to L–V immiscibility in the jadeite stability field. Shen and Keppler (1997) used a hydrothermal diamond-anvil cell to establish supercritical behavior of albite–H₂O. The topology of the rutile solubility isobars (Fig. 5) extends their results. In the liquid + vapor stability field, equilibrium requires that the Ti (and H₂O) concentrations in the liquid and vapor are constant, independent of bulk composition. In our experimental approach, analysis of that glass would return constant Ti concentration regardless of the bulk H₂O content of the system within the limits of the miscibility gap. In principle, H₂O (and albite) content of the liquid should also be constant; however, interpretation of the H₂O content inferred for the quenched glasses is ambiguous. In contrast, where only one fluid phase is stable, the Ti contents of the fluid at rutile saturation vary continuously across the binary. Notably, however, the topology of this variation must change with distance from the crest of the miscibility gap: for a system at critical mixing, the Ti concentration is nearly constant as H₂O changes; as the system is moved further into the stability field of the supercritical fluid, the rutile solubility must become more dependent on H₂O concentration. That is, the solubility isobars (Fig. 5) change from flat to sigmoidal.

Our data suggest that a single, supercritical fluid is stable from <1.0 GPa to >2.0 GPa. Fluids that quench to glass which display consistent variations in H₂O and Ti concentrations are clearly supercritical (Table 1, and Fig. 5). This behavior is prevalent at 1.0 to 2.0 GPa across the compositional range investigated. In contrast, experiments

at 0.9 and 2.2 GPa are probably very slightly subcritical. Fig. 5 shows that Ti concentrations do not change with bulk H₂O, which is required in the liquid + vapor field. That these runs in almost all cases quench to very fine glass particles is consistent with this interpretation. Thus, the transitions from detectable variation in Ti with changing H₂O, to constant Ti with H₂O, indicate the lower and upper limits of the supercritical behavior of albite–H₂O fluids (Fig. 8).

Shen and Keppler (1997) found that in the albite stability field, closure of the liquid + vapor miscibility gap occurred at 1.1 ± 0.1 GPa at 900 °C. In contrast, our interpretations above require that the crest of the liquid–vapor miscibility gap at 900 °C is ~0.9–1.0 GPa (Fig. 8). In light of uncertainties in both methods, this discrepancy is probably not significant.

Perhaps the most significant result of our experiments is that solubility isobars at $P > 1.25$ GPa progressively flatten with increasing P , and that at 2.2 GPa the isobar again indicates no dependence of rutile solubility on H₂O content. As at 0.9 GPa, this behavior must mean that the system has again returned the point of unmixing into liquid + vapor phases with rising P . Such compression-induced vapor exsolution is nominally surprising behavior in silicate–H₂O systems. Yet consideration of the phase relations in Fig. 1 shows that this observation simply confirms the existence of the high- P liquid + vapor field required by the H₂O-saturated melting behavior of jadeite + quartz. As illustrated in Fig. 8, the reappearance of a liquid + vapor field occurs a P lower than the jadeite–albite–quartz equilibrium at 900 °C. The schematic trajectory of the upper boundary of the supercritical fluid stability field sketched in Fig. 1 is unconstrained; it is not known whether it intersects the jadeite + quartz melting curve to form a stable critical point, projects to a metastable intersection in the albite stability field, or exhibits some other more complex topology. Manning (2004) and Manning et al. (2010) pointed out that supercritical mixing of silicate–H₂O system requires stabilization of polymeric Si- and Si–Al species over the binary of interest. Our finding that, with isothermal compression, albite–H₂O exhibits first a transition to supercritical behavior, and then a high- P return of the miscibility gap suggests that some combination of aluminosilicate polymer stability and coordination changes – perhaps Al, as indicated

by the change from 4-fold in albite to 6-fold in jadeite – govern the width of the supercritical fluid field.

4.4. Geologic implications

Decreasing rutile solubility with rising P in supercritical albite–H₂O fluids might initially be interpreted to suggest that deep, hot metasomatic environments may not be good candidates for Ti mobility. However, even at higher P (2.0 GPa), Ti solubility in intermediate composition fluids is significantly higher (~2000 ppm or roughly an order of magnitude) than in pure H₂O or in dilute albite–H₂O systems (Audéat and Keppler, 2005; Tropper and Manning, 2005; Antignano and Manning, 2008). Antignano and Manning (2008) concluded that raising Ti levels high enough to produce residual rutile would require a mechanism for enhancing Ti solubility that is more effective than P and T alone. This study demonstrates that supercritical fluids may be effective in enhancing rutile solubility in metasomatic fluids, and that the mobility of Ti – and therefore other HFSE – may be greater than previously thought in suitable fluid compositions.

There has been speculation about the role of supercritical fluids as possible agents of element transfer in subduction zones. To the extent that albite–H₂O fluids are useful models for this behavior, the results of this study highlight that the P – T region of this behavior may be narrower than previously recognized. Very few geothermal gradients in subduction zones would encounter the supercritical fluid field constrained by our experiments (e.g., Syracuse et al., 2010). Thus, a clearer understanding on the controls of liquid–vapor mixing at high P is required before it can be assumed that supercritical behavior is commonly achieved during subduction-zone metamorphism.

5. Conclusions

- (1) Rutile solubility was measured in the supercritical albite–H₂O system using hydrothermal piston–cylinder methods at 900 °C. Quench textures and H₂O and Ti contents of glasses indicate that the system is supercritical at $0.9 < P < 2.2$ GPa.
- (2) Ti solubility decreases with P at constant bulk H₂O and is significantly higher than in pure water or in dilute albite–H₂O systems (Antignano and Manning, 2008), confirming that dissolved Na–Al–silicate enhances Ti solubility. Solubilities are everywhere lower than previously found in hydrous melts of comparable composition (Hayden and Watson, 2007). Ti solubility increases with increased albite content of the fluid, and is on the order of ~1000 to ~5000 ppm. Solubility isobars show that Ti decreases with bulk H₂O at 1–2 GPa. The dependence is complex and sigmoidal. At 0.9 and 2.2 GPa, Ti shows no change with H₂O over a large range in H₂O.
- (3) The Ti contents of quenched glasses suggest that there is a low pressure crest of a liquid–vapor miscibility gap in the albite–H₂O system at 900 °C at 0.9–1.0 GPa, and that a supercritical fluid is stable until further and becomes stable above this pressure, until further compression induces a return to a subcritical state at 2.0–2.2 GPa.
- (4) If supercritical fluids exist in subduction zones or other high- P metasomatic environments and remain in the supercritical stability field during transport over significant distances, the results on the model albite–H₂O system support the assumption that they may be agents for transfer of Ti and other HFSE.

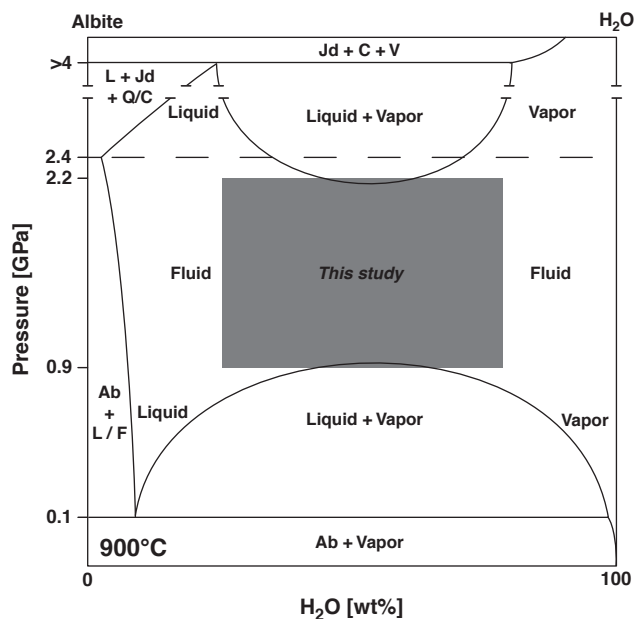


Fig. 8. Schematic isothermal pressure-composition projection for the system albite–H₂O. Pressure not to scale. Abbreviations as in Fig. 1, except: Q, quartz; C, coesite; F, fluid. The gray box illustrates the range of conditions investigated in the present study. The terminations of the liquid + vapor fields must lie very close to the lowest and highest P investigated (0.9 and 2.2 GPa, respectively). Note break in axis at high P .

Acknowledgments

This work was supported by National Science Foundation grants EAR-0711521 to CEM. The authors wish to thank Thomas Zack for his helpful review.

References

- Antignano, A., Manning, C.E., 2008. Rutile solubility in H₂O, H₂O–SiO₂, and H₂O–NaAlSi₃O₈ fluids at 0.7–2.0 GPa and 700–1000 °C: implications for mobility of nominally insoluble elements. *Chemical Geology* 255, 283–293.
- Audédat, A., Keppler, H., 2005. Solubility of rutile in subduction zone fluids, as determined by experiments in the hydrothermal diamond anvil cell. *Earth and Planetary Science Letters* 232, 393–402.
- Ayers, J.C., Watson, E.B., 1991. Solubility of apatite, monazite, zircon, and rutile in supercritical aqueous fluids with implications for subduction zone geochemistry. *Philosophical Transactions of the Royal Society of London Series A: Mathematical Physical and Engineering Sciences* 335, 365–375.
- Ayers, J.C., Watson, E.B., 1993. Rutile solubility and mobility in supercritical aqueous fluids. *Contributions to Mineralogy and Petrology* 114, 321–330.
- Baker, D.R., 2004. Piston–cylinder calibration at 400 to 500 MPa: a comparison of using water solubility in albite melt and NaCl melting. *American Mineralogist* 89, 1553–1556.
- Boettcher, A.L., Wylie, P.J., 1969. Phase relationships in the system NaAlSiO₄–SiO₂–H₂O to 35 kilobars pressure. *American Journal of Science* 267, 875–909.
- Brenan, J.M., Shaw, H.F., Phinney, D.L., Ryerson, F.J., 1994. Rutile–aqueous fluid partitioning of Nb, Ta, Hf, Zr, U and Th – implications for high-field strength element depletions in island–arc basalts. *Earth and Planetary Science Letters* 128, 327–339.
- Colasanti, C.V., Johnson, E.A., Manning, C.E., 2007. Hydrogen solubility in synthetic rutile. *Geochimica et Cosmochimica Acta* 71, A181 Supplement.
- Dickinson, J.E., Hess, P.C., 1985. Rutile solubility and titanium coordination in silicate melts. *Geochimica et Cosmochimica Acta* 49, 2289–2296.
- Dolejš, D., Manning, C.E., 2010. Thermodynamic model for mineral solubility in aqueous fluids: theory, calibration, and application to model fluid–flow systems. *Geofluids* 10, 20–40.
- Farges, F., Brown, G.E., Navrotsky, A., Gan, H., Rehr, J.J., 1996. Coordination chemistry of Ti(IV) in silicate glasses and melts: III. Glasses and melts from ambient to high temperatures. *Geochimica et Cosmochimica Acta* 60, 3055–3065.
- Force, E.R., 1991. Geology of titanium–mineral deposits. *Geological Society of America Special Paper*, 249, 112 pp.
- Gaetani, G.A., Asimow, P.D., Stolper, E.M., 2008. A model for rutile saturation in silicate melts with applications to eclogite partial melting in subduction zones and mantle plumes. *Earth and Planetary Science Letters* 272, 720–729.
- Goldsmith, J.R., Jenkins, D.M., 1985. The hydrothermal melting of low and high albite. *American Mineralogist* 70, 924–933.
- Hayden, L.A., 2007. Experimental studies of equilibrium and transport phenomena in the Earth's crust and mantle. Dissertation.
- Hayden, L.A., Watson, E.B., 2007. Rutile saturation in hydrous siliceous melts and its bearing in on Ti–thermometry of quartz and zircon. *Earth and Planetary Science Letters* 258, 561–568.
- Henderson, G.S., Liu, X.Y., Fleet, M.E., 2003. Titanium coordination in silicate glasses investigated using O K-edge X-ray absorption spectroscopy. *Mineralogical Magazine* 67, 597–607.
- Hermann, J., Spandler, C., 2008. Sediment melts at sub–arc depths. *Journal of Petrology* 49, 717–740.
- Hermann, J., Spandler, C., Hack, A., Korsakov, A.V., 2006. Aqueous fluids and hydrous melts in high–pressure and ultra–high pressure rocks: implications for element transfer in subduction zones. *Lithos* 92, 399–417.
- Holland, T.J.B., Powell, R., 1998. An internally consistent thermodynamic data set for phases of petrological interest. *Journal of Metamorphic Geology* 16, 309–343.
- Jiang, S.Y., Wang, R.C., Xu, X.S., Zhao, K.D., 2005. Mobility of high field strength elements (HFSE) in magmatic-, metamorphic-, and submarine–hydrothermal systems. *Physics and Chemistry of the Earth* 30, 1020–1029.
- Kessel, R., Schmidt, M.W., Ulmer, P., Pettker, T., 2005a. Trace element signature of subduction–zone fluids, melts and supercritical liquids at 120–180 km depth. *Nature* 437, 724–727.
- Kessel, R., Ulmer, P., Pettker, T., Schmidt, M.W., Thompson, A.B., 2005b. The water–basalt system at 4 to 6 GPa: phase relations and second critical endpoint in a K–free eclogite at 700 to 1400 °C. *Earth and Planetary Science Letters* 237, 873–892.
- Klimm, K., Blundy, J.D., Green, T.H., 2008. Trace element partitioning and accessory phase saturation during H₂O–saturated melting of basalt with implications for subduction zone chemical fluxes. *Journal of Petrology* 49, 523–553.
- Manning, C.E., 1994. The solubility of quartz in H₂O in the lower crust and upper mantle. *Geochimica et Cosmochimica Acta* 58, 4831–4839.
- Manning, C.E., 2004. The chemistry of subduction–zone fluids. *Earth and Planetary Science Letters* 223, 1–16.
- Manning, C.E., 2007. Solubility of corundum plus kyanite in H₂O at 700 °C and 10 kbar: evidence for Al–Si complexing at high pressure and temperature. *Geofluids* 7, 258–269.
- Manning, C.E., Boettcher, S.L., 1994. Rapid–quench hydrothermal experiments at mantle pressures and temperatures. *American Mineralogist* 79, 1153–1158.
- Manning, C.E., Wilke, M., Schmidt, C., Cauzzi, J., 2008. Rutile solubility in albite–H₂O and Na₂Si₃O₇–H₂O at high temperatures and pressures by in–situ synchrotron radiation micro–XRF. *Earth and Planetary Science Letters* 272, 730–737.
- Manning, C.E., Antignano, A., Lin, H.A., 2010. Premelting polymerization of crustal and mantle fluids, as indicated by solubility of albite + paragonite + quartz in H₂O at 1 GPa and 350–620 °C. *Earth and Planetary Science Letters* 292, 325–336.
- Mibe, K., Chou, I.-M., Bassett, W.A., 2008. In situ Raman spectroscopic investigation of the structure of subduction–zone fluids. *Journal of Geophysical Research* 113, B04208.
- Mysen, B.O., Ryerson, F.J., Virgo, D., 1980. The influence of TiO₂ on the structure and derivative properties of silicate melts. *American Mineralogist* 65, 1150–1165.
- Newton, R.C., Manning, C.E., 2007. Solubility of grossular, Ca₃Al₂Si₃O₁₂, in H₂O–NaCl solutions at 800 °C and 10 kbar, and the stability of garnet in the system CaSiO₃–Al₂O₃–H₂O–NaCl. *Geochimica et Cosmochimica Acta* 71, 5191–5202.
- Newton, R.C., Manning, C.E., 2008. Solubility of corundum in the system Al₂O₃–SiO₂–H₂O–NaCl at 800 °C and 10 kbar. *Chemical Geology* 249, 250–261.
- Rudnick, R.L., Barth, M., Horn, I., McDonough, W.F., 2000. Rutile-bearing refractory eclogites: missing link between continents and depleted mantle. *Science* 287, 278–281.
- Ryerson, F.J., Watson, E.B., 1987. Rutile saturation in magmas: implications for Ti–Nb–Ta depletion in island–arc basalts. *Earth and Planetary Science Letters* 86, 225–239.
- Schuing, R.D., Vink, B.W., 1967. Stability relations of some titanium–minerals (sphene, perovskite, rutile, anatase). *Geochimica et Cosmochimica Acta* 31, 2399–2411.
- Shen, A.H., Keppler, H., 1997. Direct observation of complete miscibility in the albite–H₂O system. *Nature* 385, 710–712.
- Spandler, C., Mavrogenes, J., Hermann, J., 2007. Experimental constraints on element mobility from subducted sediments using high–P synthetic fluid/melt inclusions. *Chemical Geology* 239, 228–249.
- Stadler, R., Ulmer, P., Thompson, A.B., Günther, D., 2000. Experimental approach to constrain second critical end points in fluid/silicate systems: near–solidus fluids and melts in the system albite–H₂O. *American Mineralogist* 85, 68–77.
- Syracuse, E.M., van Keken, P.E., Abers, G.A., 2010. The global range of subduction zone thermal models. *Physics of Earth and Planetary Interiors* 183, 73–90.
- Tropper, P., Manning, C.E., 2005. Very low solubility of rutile in H₂O at high pressure and temperature, and its implications for Ti mobility in subduction zones. *American Mineralogist* 90, 502–505.
- van Baalen, M.R., 1993. Titanium mobility in metamorphic systems: a review. *Chemical Geology* 110, 233–249.
- Zack, T., Kronz, A., Foley, S.F., Rivers, T., 2002. Trace element abundances in rutiles from eclogites and associated garnet mica schists. *Chemical Geology* 184, 97–122.